### RESEARCH ARTICLE



Check for updates

# In vitro and in vivo degradation correlations for polyurethane foams with tunable degradation rates

Anand Utpal Vakil<sup>1</sup> | Natalie Marie Petryk<sup>1</sup> | Changling Du<sup>1</sup> |
Bryanna Howes<sup>2</sup> | Darnelle Stinfort<sup>3</sup> | Serenella Serinelli<sup>4</sup> | Lorenzo Gitto<sup>4</sup> |
Maryam Ramezani<sup>1</sup> | Henry T. Beaman<sup>1</sup> | Mary Beth Browning Monroe<sup>1</sup>

#### Correspondence

Mary Beth Browning Monroe, Department of Biomedical and Chemical Engineering, BioInspired Syracuse, Institute for Materials and Living Systems, Syracuse University, 318 Bowne Hall, Syracuse, NY 13244, USA. Email: mbmonroe@syr.edu

#### **Funding information**

Air Force Research Laboratory, Grant/Award Number: FA8650-18-2-6978

#### **Abstract**

Polyurethane foams present a tunable biomaterial platform with potential for use in a range of regenerative medicine applications. Achieving a balance between scaffold degradation rates and tissue ingrowth is vital for successful wound healing, and significant in vivo testing is required to understand these processes. Vigorous in vitro testing can minimize the number of animals that are required to gather reliable data; however, it is difficult to accurately select in vitro degradation conditions that can effectively mimic in vivo results. To that end, we performed a comprehensive in vitro assessment of the degradation of porous shape memory polyurethane foams with tunable degradation rates using varying concentrations of hydrogen peroxide to identify the medium that closely mimics measured in vivo degradation rates. Material degradation was studied over 12 weeks in vitro in 1%, 2%, or 3% hydrogen peroxide and in vivo in subcutaneous pockets in Sprague Dawley rats. We found that the in vitro degradation conditions that best predicted in vivo degradation rates varied based on the number of mechanisms by which the polymer degraded and the polymer hydrophilicity. Namely, more hydrophilic materials that degrade by both hydrolysis and oxidation require lower concentrations of hydrogen peroxide (1%) to mimic in vivo rates, while more hydrophobic scaffolds that degrade by oxidation alone require higher concentrations of hydrogen peroxide (3%) to model in vivo degradation. This information can be used to rationally select in vitro degradation conditions that accurately identify in vivo degradation rates prior to characterization in an animal model.

#### **KEYWORDS**

degradation, foams, polyurethane, shape memory polymers

# 1 | INTRODUCTION

The use of degradable biomaterial scaffolds for tissue regeneration allows cells surrounding the implant site to attach, proliferate, and generate new tissue as the scaffold degrades away.<sup>1-7</sup> This

approach can eliminate complications associated with scaffold removal after healing. Thus, matching scaffold degradation and tissue regeneration rates is crucial for effective regeneration. Scaffold degradation that is too slow relative to tissue regeneration can hinder growth of new blood vessels and tissues, while degradation

This is an open access article under the terms of the Creative Commons Attribution-NonCommercial License, which permits use, distribution and reproduction in any medium, provided the original work is properly cited and is not used for commercial purposes.

© 2023 The Authors. Journal of Biomedical Materials Research Part A published by Wiley Periodicals LLC.



<sup>&</sup>lt;sup>1</sup>Department of Biomedical and Chemical Engineering and BioInspired Syracuse, Institute for Material and Living Systems, Syracuse University, Syracuse, New York, USA

<sup>&</sup>lt;sup>2</sup>Department of Chemistry, Le Moyne College, Syracuse, New York, USA

<sup>&</sup>lt;sup>3</sup>Biotechnology Program, Syracuse University, Syracuse, New York, USA

<sup>&</sup>lt;sup>4</sup>SUNY Upstate Medical University, Syracuse, New York, USA

Society For WILEY 581

that is too rapid could cause scaffold failure before adequate tissue scaffolding is in place.

In biodegradable scaffolds, the diffusion of nutrients and oxygen can be improved by incorporating interconnected pores.<sup>8,9</sup> Furthermore, the ability to safely implant scaffolds is crucial, particularly in irregularly shaped defects. Effective implantation can be achieved with porous shape memory polymers (SMPs). A porous SMP scaffold can be initially deformed and stored in a low-profile shape that is easy to implant. Upon implantation, scaffold expansion could be triggered by heating to body temperature and exposure to water to enable recovery to the original shape and filling of the wound space.

One system with promise for use in regenerative medicine is highly crosslinked thermoset polyurethane SMP foams. These low-density SMP foams have a high volume recovery ratios and tunable recovery rates. Additionally, their exceptional chemical and physical tunability and high biocompatibility make polyurethane SMPs an attractive option for various biomedical applications. The degradation mechanism of these polyurethane SMPs was initially demonstrated by Weems et al. Tertiary amines in the polyol monomers undergo oxidative degradation, and the materials are exceptionally resistant to hydrolytic degradation.

Several others have tried to further control polyurethane SMP foam degradability. Hydrolytically degradable ester linkages were incorporated using poly(\varepsilon-caprolactone) (PCL). 14 While degradation could be tuned with PCL, the overall degradation rate was slow, and the foams had a low glass transition temperature (Tg, <25°C) that limits their practical use in terms of storing materials in their secondary shapes. 14 A faster degradation rate (80% mass loss over 80 days in 2% H2O2) was achieved by incorporating succinic acid-based esters into SMP foams. 15 However, this system required heating to 50°C to achieve complete volume expansion, thus necessitating the use of an external heating mechanism to actuate these SMPs post-implantation. Other work by Jang, et al. employed ester-containing monomers to improve thermal and shape memory properties, but this system also degraded slowly. 16 In our recent work, we incorporated esters formed by the reaction between nitrilotriacetic acid (NTA) and diethylene glycol (DEG) to increase the degradation rate (100% mass loss within 30 days in 3% H<sub>2</sub>O<sub>2</sub>) while maintaining thermal and shape memory properties.<sup>17</sup>

There have also been efforts to slow degradation and obtain biostable SMP foams by replacing tertiary amine-containing polyols with glycerol, isocyanurate, and hexanetriol.  $^{18-20}$  In our recent work, we increased the biostability of porous SMP foams by incorporating diethylene glycol (DEG).  $^{21}$  This approach slowed the degradation rate to provide materials with 20% mass remaining after 102 days in 3%  $\rm H_2O_2.^{21}$  Slowly degrading SMP foams could be valuable for long-term implants and/or for applications in which the material is removed and no degradation is desired prior to explantation.

Multiple animal models have demonstrated the healing capabilities of these SMP foams. In a porcine aneurysm model by Rodriguez et al., almost complete penetration of collagen through the foam volume, lack of inflammation, and a thick fibrous cap across the aneurysm neck were observed at 90 days, demonstrating foam biocompatibility.<sup>22</sup> A SMP foam-coated metal coil was used by Horn et al. to treat a porcine sidewall aneurysm.<sup>23</sup>

Approximately 89%–93% reduction in the cross-sectional aneurysm area was observed over 180 days after SMP foam treatment, indicating long-term healing capabilities. Weems et al. later cleaned the explanted material from aneurysms and qualitatively characterized degradation using spectroscopy. It was concluded that the in vivo mass loss profile was much slower than that obtained in vitro using a 3%  $H_2O_2$  solution, which is generally considered to be "real-time" oxidation media. Degradation of SMP foams via multinucleated giant cells with subsequent fibrin deposition was characterized via histological assessment by Jessen et al. using a porcine vascular occlusion model. In this model, a steady, but slow degradation rate of  $\sim$ 3% mass loss/30 days was estimated using cross-sectional area measurements of foam histology images.

In sum, multiple approaches have been used to synthesize SMP foams with desirable physical and shape memory properties and tunable degradation rates. However, there has been inconsistency in in vitro characterization in terms of degradation media selection (e.g.,  $\rm H_2O_2$  concentration), and focused in vivo characterization of SMP foam degradation is limited. It is vital to develop a reliable method for obtaining in vivo degradation profiles of SMP foams while confirming their safety. This method could also be useful for comparing degradation profiles of selected formulations with data that is provided in the literature to rationally select materials with desired degradation outcomes.

Here, porous SMP foams with previously established in vitro degradation rates were utilized, and their in vivo degradation profiles were assessed in a subcutaneous rat model over 12 weeks. This animal model is often used to evaluate biomaterial scaffold degradation and host response over time, providing a clear point of comparison with previously characterized biomaterials.<sup>26-31</sup> Since previous work has shown that in vitro methods fail to accurately predict in vivo degradation profiles, samples were subjected to in vitro oxidative degradation with reduced processing as compared with literature-reported methods. 13,32 Also, varying concentration of H<sub>2</sub>O<sub>2</sub> (1%, 2%, and 3%) were used to identify the medium that most closely predicted in vivo degradation profiles. While a subset of these materials contain ester linkages that are susceptible to hydrolysis by water and/or enzymatic degradation by lipase, we focused on oxidative media here based on our prior data showing high hydrolytic stability. 17 To complement histological assessments, in vitro cytotoxicity analysis of fully degraded samples was performed to assess material safety.<sup>33</sup> These studies provide fundamental information on correlating in vivo and in vitro degradation profiles, expanding the characterization of a valuable biomaterial system. This information could be further used to improve the rational in vitro characterization of other degradable biomaterials prior to their use in animals.

# 2 | MATERIALS AND METHODS

#### 2.1 | Materials

NTA, DEG, 1-(3-dimethyl aminopropyl)-3-ethyl carbodiimide HCl (EDC), 4-(dimethylamino) pyridine (DMAP,  $\geq$  99%), N,N,N',N'-tetra-kis-2-hydroxypropyl ethylenediamine (HPED), triethanol amine (TEA), hexamethylene diisocyanate (HDI), chloroform, ethanol,

acetone, isopropyl alcohol, Triton X-100, phosphate-buffered saline (PBS), and trypsin were purchased and used as received from Fisher Scientific (Waltham, MA, USA). Collagenase (clostridium histolyticum) and pancreatin (porcine pancreas) were purchased from Sigma Aldrich and used as received. Surfactant EPH-190 and catalysts T-131 and BL-22 were used as received from Evonik (Essen, Germany).

#### 2.2 | SMP foam fabrication and characterization

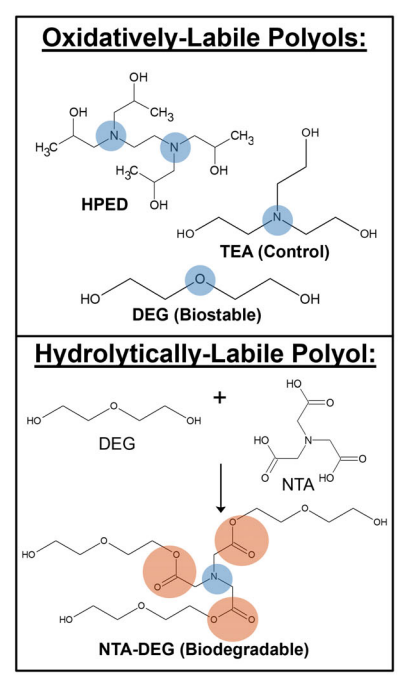
### 2.2.1 | Ester-containing monomer synthesis

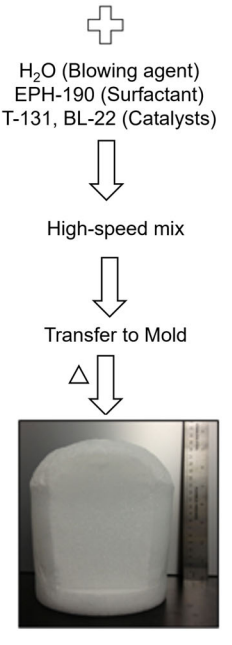
The ester-containing monomer, NTA-DEG, was synthesized as previously described. Priefly, NTA was initially dissolved in chloroform with 0.1 mol. eq. of DMAP. Once all components were completely dissolved, DEG was added dropwise at ratio of 1:3 (NTA:DEG). Then, EDC was added at a ratio of 1:3 (NTA:EDC). The reaction proceeded at 40°C for 24 h. The reaction was tracled via attenuated total reflectance-Fourier transform infrared spectroscopy (ATR-FTIR, Nicolet, Fisher Scientific, Waltham, MA, USA) to confirm the appearance of the C=O ester peak at ~1741 cm<sup>-1</sup>. After completion, excess solvent was evaporated using rotary evaporation and the product was dried overnight under –30 in Hg vacuum at 40°C. 1H Nuclear magnetic resonance spectroscopy (NMR, Avance III HD 400 MHz, Bruker) was performed on the product as previously described to confirm ~85%-88% functionalization of NTA carboxylic acids with DEG. 17

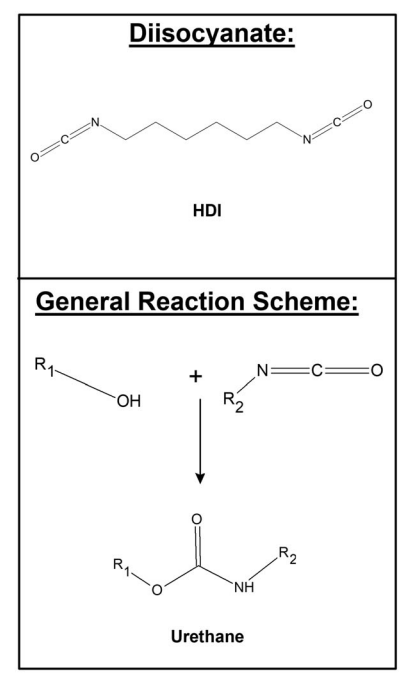
### 2.2.2 | Foam synthesis

Foams were prepared as previously described. 17,21 First. all required isocyanate equivalents provided by HDI were mixed with 35% of the required hydroxyl equivalents (HPED with TEA, DEG, or NTA-DEG) under an inert dry atmosphere in a glovebox (Labconco, Kansas City, MO, USA). This mixture (premix) was cured at 50°C for 48 h. Then, surfactant was added to the premix and mixed at 3500 rpm using a speed mixer (Flacktek, Landrum, SC, USA) for 30 s before cooling to room temperature. The second component (hydroxyl [OH] mix) was prepared parallelly with the balance hydroxyls (HPED, NTA-DEG, water, and/or TEA) along with catalysts (T-131 and BL-22). The OH mix components were mixed in a speed mixer at 3500 rpm for 30 s and added to the premix container. Both components were then mixed at 1800 rpm for 5 s and poured into a 1-L container to allow for foaming at 50°C for 10 min. The foam was kept in a fume hood overnight to ensure complete reaction. A schematic of foam formation is shown in Figure 1, and Table 1 contains details on the components of synthesized foams. All samples were initially cleaned twice in deionized water and twice in 70% ethanol, alternatively for 15 min each.

The surface chemistry of synthesized samples was analyzed using ATR-FTIR after synthesis and throughout degradation. The characteristic peaks identified to confirm successful synthesis and monitor degradation include carbonyl of urethane at  $\sim\!1680~\text{cm}^{-1}$ , carbonyl of ester at  $\sim\!1730~\text{cm}^{-1}$ , ether at  $\sim\!1090~\text{cm}^{-1}$ , and tertiary amines at  $\sim\!1050~\text{cm}^{-1}$ .







Esters: Hydrolytic degradation in water Tertiary amines: Oxidative degradation in H<sub>2</sub>O<sub>2</sub>

**TABLE 1** Synthesized foam compositions

Sample name	HDI (wt%)	HPED (wt%)	TEA (wt%)	DEG (wt%)	NTA-DEG (wt%)	EPH 190 (wt%)	T-131 (wt%)	BL-22 (wt%)	Water (wt%)
Control	54.03	27.61	8.05	-	_	6.44	0.46	1.01	2.37
30% DEG	53.16	27.15	-	8.69	-	6.19	0.60	1.18	2.91
30% NTA-DEG	43.10	24.40	-	-	21.71	6.17	1.10	1.23	2.29

### 2.2.3 | Pore size analysis

Thin slices (1 cm width, 1 cm length, and 0.5 cm height) were cut from washed foams along the longitudinal and horizontal axes. The slices were sputter coated (Desk V Sputter coater, Denton Vacuum, Moorestown, NJ, USA) with a layer of gold for 45 s under vacuum. Samples were mounted onto a holder, and pore morphology was analyzed using scanning electron microscopy (SEM, JSM 5600, JEOL, Peabody, MA, USA) at  $35 \times$  magnification and an accelerating voltage of 10 kV. Pore size was quantified as the largest diameter of all visible pores in an image using ImageJ.

### 2.2.4 | Density and surface area

Foam density (n=3) was measured by cutting samples into small cubes with each side measuring  $\sim 1$  cm and weighing them. The length of each face of the sample was measured using calipers and volume was recorded as length  $\times$  width  $\times$  height. Sample weight was divided by the volume to determine the average density of foams.

Surface area was calculated using a previously determined correlation between specific surface area and pore size of polyurethane foams, Equation (1). $^{13}$  Slope (20.91944 ± 0.312) and intercept ( $-11.34565 \pm 0.406$ ) were previously obtained by plotting specific surface area (mm $^2$ /mm $^3$ ) against known pore size (mm) for each pore. Then, average surface area of samples was calculated using density and specific surface area based on Equation (2).

$$\label{eq:Specific surface area} Specific surface area \left(\frac{mm^2}{mm^3}\right) = \left(\text{Pore size}\left(\text{mm}\right) \times \text{slope}\right) + \text{intercept,}$$
 
$$\tag{1}$$

Surface area 
$$\left(\frac{cm^2}{g}\right) = \frac{\text{Specific surface area}\left(\frac{mm^2}{mm^3}\right)}{\text{Density}\left(\frac{g}{cm^3}\right)} \times 10\left(\frac{mm}{cm}\right), \quad (2)$$

#### 2.2.5 | Hydrophilicity

Thin slices of nonporous films were prepared from the same compositions listed in Table 1 without the addition of surfactant or water (blowing agent). The contact angle was measured using a goniometer (Model 500, Ramé-hart Co, Succasunna, NJ). Water (2 ml, n=6) was dropped onto each film, and images were captured at a 0.01-s interval (SuperSpeed U4 series). Images were analyzed using DROPImage software to determine the contact angle between the water droplet and the film.

# 2.2.6 | Thermal and mechanical analysis

To measure glass transition temperature ( $T_{\rm g}$ ), samples (n=3) were cut into thin slices (3–5 mg) and loaded into t-zero aluminum pans with lids. Pans were placed onto DSC Q200 (TA Instruments, New Castle, DE, USA), equilibrated at  $-40^{\circ}$ C, held isothermally for 2 min, heated to 120°C at  $10^{\circ}$ C/min, held isothermally for 2 min, cooled to  $-40^{\circ}$ C at  $-10^{\circ}$ C/min, held isothermally for 2 min, and heated back to  $120^{\circ}$ C at  $10^{\circ}$ C/min. The half-height transition temperature of the endothermic shift during the second heating cycle was recorded as dry  $T_{\rm g}$ .

To measure the wet  $T_{\rm g}$ , samples (n=3, 3–5 mg) were placed in water at 50°C for 12 min and then loaded in t-zero aluminum pans with hermetic lids. Samples were equilibrated at -60°C, held isothermally for 2 min, heated to 100°C at 10°C/min, and held isothermally for 2 min. Wet  $T_{\rm g}$  was recorded as the half-height transition temperature during the endothermic shift in the single heating cycle.

Samples (n=5) were cut into dog bones (ASTM D638 scaled down by a factor of 4) with a gauge length of 6.25 mm and width of 1.5 mm. The thickness of each sample was measured, and then samples were subjected to a tensile force (Test Resources, Shakopee, MN, USA) via a 24 N load cell. The tensile force was applied at 2 mm/min until failure, and the resulting stress/strain curve was used to measure elastic modulus, ultimate tensile strength, and elongation at break. To test samples in wet conditions, they were placed in deionized water at  $50^{\circ}$ C for 1 h prior to testing.

# 2.2.7 | Shape memory behavior

Cylindrical samples (diameter = 8 mm, length = 1 cm) were threaded onto a nitinol wire (diameter = 330  $\mu m$ ) longitudinally. Samples were heated to  $70^{\circ} C$  for 10 min (i.e., above their  $T_g$ ), crimped radially (Blockwise Engineering, Tempe, AZ, USA), and cooled in the crimper for 15 min at room temperature. The crimped volume was measured using calipers. Samples were placed in an airtight container for 24 h and the crimped volume was measured again to determine shape fixity (Equation 3). Then, samples were placed in a water bath at  $37^{\circ} C$  for 10 min, and images were captured every 5 s. ImageJ was used to measure sample volume at each time point (t) and determine volume recovery (Equation 4).

$$\label{eq:Shape fixity} Shape fixity (\%) = 1 - \frac{\text{Crimped volume}_{2^4\,h} - \text{Crimped volume}_{0\,h}}{\text{Crimped volume}_{0\,h}} \times 100\%, \tag{3}$$

$$Volume\ recovery\ (\%) = \frac{Sample\ volume\ (t)}{Expanded\ volume} \times 100\%, \tag{4}$$



# 2.3 | Cytocompatibility

# 2.3.1 | Indirect cytocompatibility

After cleaning, samples were soaked in sterile PBS overnight to ensure complete removal of ethanol and placed in Transwell® inserts in preseeded 24-well plates containing NIH mouse fibroblast 3T3 cells (10,000 cells per well) that had been cultured for 24 h in Dulbecco's Modified Eagle Medium (DMEM) with 10% fetal bovine serum (FBS) and 1% penicillin–streptomycin (PS) at 37°C. This study indirectly measures potential effects of foam leachables in the media on cell viability and is useful for biomaterials that do not have specific attachment sites for cells. Wells that contained empty inserts were used as positive cytocompatible controls. Negative cytotoxic controls included wells with 0.5% H<sub>2</sub>O<sub>2</sub> added to cause cell death. At 3, 24, and 72 h, Transwell inserts and samples were removed from the wells, and media was replaced with Resazurin cell viability stain for 2 h at 37°C before measuring fluorescence at 570 nm using a microplate reader (FLx900, Bio-Teck Instruments Inc). Cell viability was measured according to Equation (5):

$$Cell \ viability (\%) = \frac{Abs_{570}(x)}{Abs_{570}(Control)} \times 100\%, \tag{5}$$

where *x* is the selected treatment group, and the cytocompatible empty insert control was used as a standard with 100% viability.

# 2.3.2 | Foam degradation byproduct cytocompatibility

To test degradation byproduct cytocompatibility, cylindrical foams (8 mm diameter, 1 cm length) were completely degraded in 15 ml of 30%  $\rm H_2O_2$  at 70°C. Media was regularly replenished. The solutions were then diluted to 2%  $\rm H_2O_2$ , and  $\rm H_2O_2$  was neutralized using catalase (1500 U/ml) for 7 days at 37°C. Complete neutralization was confirmed using a ferric thiocyanate kit (Chemetrics). The concentration of remaining catalase was measured using Pierce Coomassie Plus Protein Assay (ThermoFisher Scientific, Waltham, MA, USA). The solutions were then filtered (0.22  $\mu$ m) and serially diluted in cell culture media to analyze cytocompatibility. The solutions were placed on top of 3T3 mouse fibroblasts pre-seeded in wells for 24 h as described above. At 3 h, cell viability was measured relative to media-only controls using the resazurin assay and Equation (5).

#### 2.4 | Degradation characterization

# 2.4.1 | In vitro degradation profiles

Varying concentrations of  $H_2O_2$  (1%, 2%, and 3%) were prepared to analyze in vitro degradation profiles at  $37^{\circ}$ C. Cylindrical samples (diameter = 8 mm, length = 1 cm) were incubated in 15 ml of media. To replicate previous work, one sample set was used throughout the entire degradation process.  $^{13,16,17,21}$  Samples were removed from media, washed in 70% ethanol, dried under vacuum at  $40^{\circ}$ C, weighed,

and then returned to fresh media for continued analysis. This technique is referred to as the "Literature Method." To compare the effects of repeated washing/drying, a parallel study was carried out in which unique samples sets were prepared for each time point. Weights of these sacrificial samples were recorded after washing and drying and then samples were removed from the study. This technique is referred to as the "Optimized Method." In both studies, degradation media was replaced twice per week, and samples were characterized at 1, 2, 3, 4, 6, and 12 weeks in terms of pore size (Section 2.2.3), thermal (Section 2.2.5), and spectroscopic (Section 2.2.2) properties.

#### 2.4.2 | Sterilization

Cleaned cylindrical (diameter = 8 mm, length = 1 cm) samples were sterilized via UV-C light (UV sterilizer cabinet, Skin Act, Pacoima, CA, USA) at 240 nm for 4 h. Samples were characterized in terms of mass,  $T_{\rm g}$ , pore size, and surface chemistry to measure effects of sterilization on foam properties, Figure S1.

#### 2.4.3 | Surgical procedure

All procedures were performed per policies set by Syracuse University's Institutional Animal Care and Use Committee (IACUC) under the guidance provided by the American Veterinary Medical Association (AVMA). A total of 36 female Sprague Dawley rats, aged at 11 weeks were selected to enable comparison with previous studies. <sup>35–40</sup> Rats were anesthetized using 2% inhalation isoflurane with oxygen at 2 ml/min, and anesthesia was maintained throughout the procedure. Incision sites (two per rat) were trimmed to remove fur and cleaned using skin cleanser (chlorhexidine gluconate) and isopropyl alcohol. Four subcutaneous pockets were created (two per side), and sterilized samples were implanted into each subcutaneous pocket using forceps. The implantation location for each sample was rotated amongst the ventral and lateral locations. Incision sites were closed using wound clips (5 mm, Braintree Scientific) and cleaned using isopropyl alcohol.

#### 2.4.4 | Post-operative procedure

Bupivacaine (0.1 ml) was placed on incision sites once a day for 72 h as a pain reliever. A subset (six) of rats were sacrificed at each time point – 1, 2, 3, 4, 6, and 12 weeks—via  $CO_2$  asphyxiation according to AVMA guidelines. Cervical dislocation was performed before explanting samples from each rat. Out of the samples collected, five samples per each formulation were used for ex vivo characterization while one sample was preserved in 4% formaldehyde and shipped to Histowiz® (Brooklyn, NY, USA) for histological staining.

# 2.4.5 | Ex vivo sample characterization

Post explantation, samples were cleaned to remove attached tissue and blood as described by Zhang et al.<sup>41</sup> Samples were subjected to

three 24 h enzyme washes over 72 h. The enzyme solution contained equal parts of collagenase (500 units/mL buffer), pancreatin (0.5 g/100 ml buffer), and trypsin (0.5%). Samples then underwent 4, 6-hour washes in 10% Triton X-100 and 8, 3-h washes in deionized water. Non-implanted samples were subjected to the same washing procedure as a control. Washed samples were characterized in terms of mass loss,  $T_{\rm g}$ , pore structure, and surface chemistry. Minimal differences were found in non-implanted sample masses before and after washing, Figure S2. Pore sizes of control and DEG foams were reduced after washing, and  $T_{\rm g}$  of control foams was reduced. No notable changes in surface chemistry were found in FTIR. Overall, the enzyme wash had small effects on foam properties; however, due to the changes that were measured, washed foams were used as controls to ensure that the enzyme wash was accounted for in the in vivo versus in vitro degradation measurements.

### 2.4.6 | Histological assessment

Samples were sectioned along their longitudinal axis, stained with hematoxylin and eosin (H&E), placed in immersion oil, and scanned via 100× objective. To avoid bias, a blind assessment of resulting images was performed by two pathologists. Collagen deposition was measured in each sample by analyzing collagen density and organization (none, intermediate, and high density/organization). A debris score of none, minimal, mild, moderate, and severe was assigned based on the amount of residual fibrin, hemorrhage, and necrosis observed in each sample. 12 Surrounding tissues were ranked based on the level of inflammation observed. Individual inflammatory cells were counted in nine high power fields (HPFs, defined as  $\sim 0.01 \text{ mm}^2$ ) per sample. Inflammatory cell types that were identified and counted included neutrophils, lymphocytes, eosinophils, plasma cells, and macrophages (including giant cells, erythrophagocytic cells, and hemosiderin-laden macrophages). Each implant was then given an overall tissue response score based on inflammation, neovascularization, and ECM content analysis.<sup>25</sup>

# 2.5 | Statistical analysis

Measurements are presented as mean ± standard deviation. The number of measurements were maintained at three for all analysis. Statistical analysis was performed by one-way analysis of variance and

Tukey's post-hoc test (2-sample, assuming unequal variance) using Microsoft Excel as mentioned in each figure legend. Statistical significance was accepted as p < .05.

### 3 | RESULTS AND DISCUSSION

#### 3.1 Density, pore structure, and surface area

As shown in Table 2, all foams had comparable pore sizes of  $\sim\!1100-1300~\mu m$ , which enables comparison with previously published SMP foam degradation results.  $^{13,16}$  Open pores with high interconnectivity were observed in DEG and NTA-DEG foams, while control foams had relatively closed pores, as shown in Figure 6. This increased interconnectivity along with sufficiently large pores would allow for nutrient and waste transport and tissue and blood vessel ingrowth during the wound healing stages.  $^{42,43}$  Low target densities well below 0.1 g/cm³ were obtained in all foams. These highly porous, low-density foams can be crimped into smaller constricted geometries during shape fixation, which would enable easy implantation. Increased surface areas were observed in foams with larger pores and lower densities, with the highest surface area calculated for 30% DEG foams.

#### 3.2 | Thermomechanical properties

The contact angle measured on each film followed expected trends based on monomer chemistries, Table 2. The highest contact angle (87°) was observed on the control formulation, while 30% DEG had a slightly lower contact angle of 61° due to the hydrophilic ether linkages. Ester-containing 30% NTA-DEG had the lowest contact angle (52°) due to increased hydrophilicity provided by esters and ethers

Dry  $T_{\rm g}$  was above 40°C for all formulations, Table 3. A dry  $T_{\rm g}$  above room temperature ensures that SMP samples can be stably stored in their secondary shape at ambient conditions without undergoing premature actuation before the intended time of usage. In this system, heat-induced plasticization is utilized during programming and shape fixing. The polymers are heated above their  $T_{\rm g}$  in the dry state, which breaks hydrogen bonds between urethane linkages to make foams soft and malleable and enable compression into the temporary shape. Subsequent cooling of compressed foams

**TABLE 2** Physical characterization of foam pore size, density, surface area, contact angle, shape recovery (time to 100% volume expansion in 37°C water), and shape fixity

Sample	Pore size (µm)	Density (g/cm³)	Surface Area (cm <sup>2</sup> /g)	Contact angle (°)	Time to 100% volume recovery (s)	Shape fixity (%)
Control	1100 ± 300	0.045 ± 0.001	1857 ± 431	87 ± 3	230 ± 80	92 ± 6
30% DEG	1300 ± 200*	0.027 ± 0.002*	22,727 ± 217*	61 ± 4*	190 ± 10*	91 ± 5
30% NTA-DEG	1100 ± 100	0.026 ± 0.005*	3466 ± 617*	52 ± 2*	40 ± 20*	86 ± 2

Note: n = 6 for pore size, density, surface area, and contact angle. n = 3 volume recovery and shape fixity. Mean  $\pm$  standard deviation displayed. \*p < .05 relative to control foam.

**TABLE 3** Thermal and mechanical properties of shape memory polymer foams

	Dry conditions				Wet conditions			
Sample	Elastic modulus (kPa)	Ultimate tensile strength (kPa)	Ultimate elongation (%)	T <sub>g</sub> (°C)	Elastic modulus (kPa)	Ultimate tensile strength (kPa)	Ultimate elongation (%)	T <sub>g</sub> (°C)
Control	3200 ± 1700	530 ± 230	20 ± 10	53 ± 2	150 ± 20	55 ± 20	40 ± 20	30 ± 2
30% DEG	140 ± 40*	90 ± 30*	240 ± 70*	45 ± 2*	32 ± 6*	40 ± 10*	170 ± 40*	22 ± 3
30% NTA-DEG	80 ± 30*	90 ± 10*	140 ± 60*	40 ± 2*	15 ± 3*	70 ± 20*	450 ± 130*	29 ± 1

Note: n = 5 for all mechanical measurements. n = 3 for glass transition temperature ( $T_g$ ) measurements. Mean  $\pm$  standard deviation displayed. \*p < .05 relative to control.

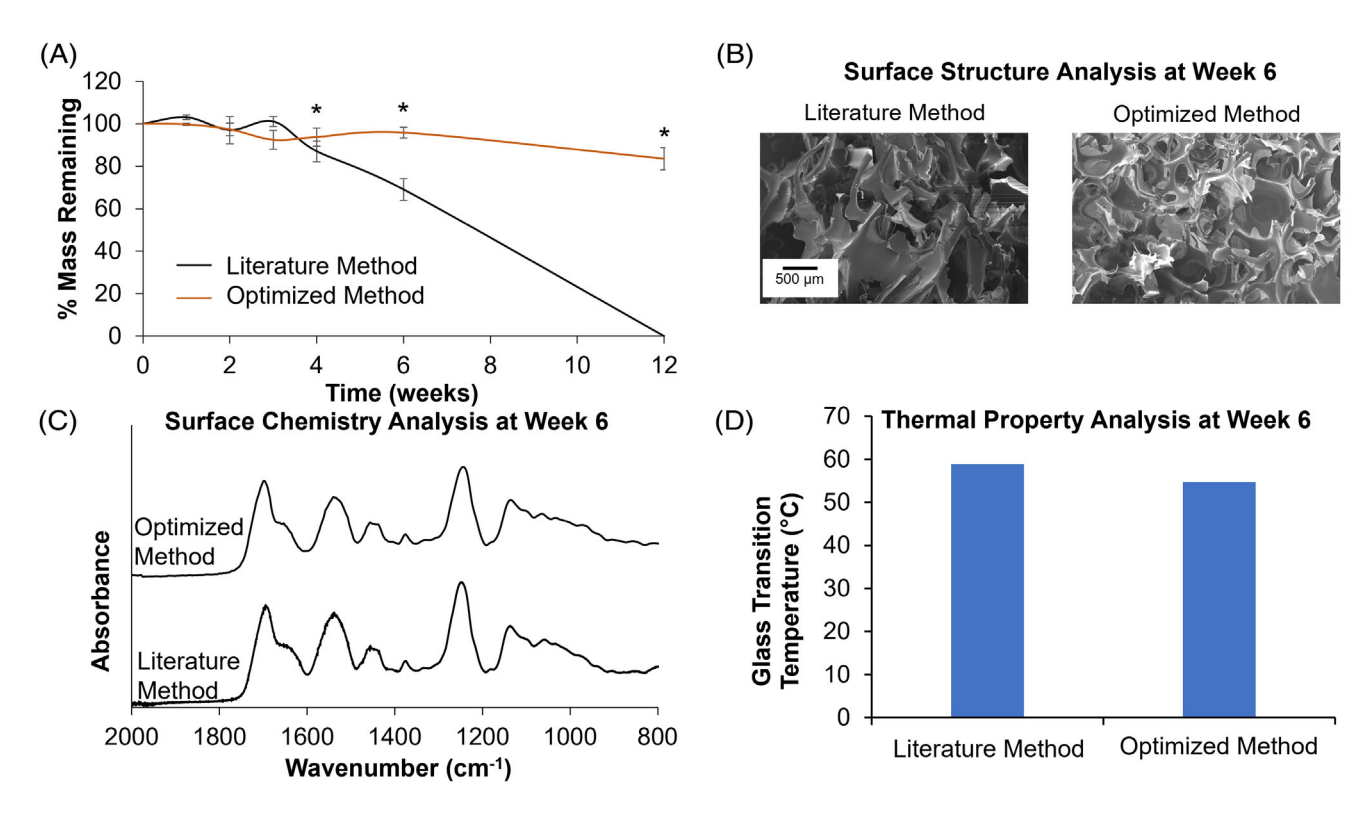


**FIGURE 2** Comparison between literature method (re-testing samples at each time point) and optimized method (testing sacrificial samples once at set time points) of in vitro degradation characterization in terms of (A) mass loss (n = 3), (B) pore structure, (C) surface chemistry, and (D) thermal properties (n = 1) of control foams. for \*p < .05 between methods

allows for formation of new hydrogen bonds between deformed chains to fix the shape in the required geometry. This shape memory behavior enables foam storage in a temporary, deformed state before implantation. A low-profile shape facilitates the application of foams to narrow or irregularly shaped wounds and/or delivery of foams via catheter. This property has been harnessed in previous in vitro and in vivo models to demonstrate that SMP foams can be easily implanted into the body. Here, all foams had high shape fixity (>85%) over 24 h of storage at room temperature, with general decreases in shape fixity with increased hydrophilicity, Table 2. This result is attributed to more hydrophilic foams absorbing ambient water during storage.

Wet  $T_{\rm g}$  below body temperature ensures that samples can passively recover their original shape once exposed to water after implantation in the body within the required time frame, Table 3. In

general, compressed foams recover their shape when the switching segments (hydrogen bonds between the urethane linkages) are broken, either by heating above the  $T_{\rm g}$  in the dry state or by water-induced plasticization and heating above the reduced wet  $T_{\rm g}$ . In these studies, plasticization and subsequent volume recovery occurred within 4 min in across all formulations in in vitro tests in 37°C water, Table 2. Faster volume recovery in NTA-DEG and DEG foams is attributed to higher hydrophilicity that enables faster water penetration, thereby reducing the time required to plasticize the network and induce shape recovery. An open pore structure also facilitates water penetration in the NTA-DEG foams, which had the fastest volume recovery. If these materials were exposed to water in the body after implantation, a fast volume recovery ensures that foams can rapidly expand to their original shape and seal wounds. This feature has potential benefit in a number of healing

Society For Biomaterials—WILEY 587

applications, such as gunshot wounds that are narrower on the outside and larger towards the inner sides.<sup>46</sup>

Table 3 shows tensile properties of samples in dry and wet conditions as an indication of properties before and after implantation, respectively. Control foams had the highest elastic modulus and tensile strength and lowest elongation under dry conditions, which is attributed to increased crosslinking in the network due to the trifunctional polyols with shorter arms (as compared with diols in DEG foams and triols with longer arms in NTA-DEG foams, Figure 1). As expected, modulus and strength decreased and elongation generally increased in wet conditions, due to softening of SMP foams after water plasticization. DEG and NTA-DEG foams had wet elastic modulus values <30 kPa, which is comparable that of human forearm skin (40 kPa)<sup>47</sup> and of subcutaneous rat tissue (65 kPa).<sup>48</sup> Lower stiffness ensures that samples do not impart unwanted stress onto the surrounding tissues after expanding within the wound site into which they are implanted.

# 3.3 | Degradation analysis: in vitro and in vivo correlations

# 3.3.1 | In vitro protocol refinement

During prior in vitro studies in 3%  $\rm H_2O_2$ , 30% NTA-DEG foams underwent complete mass loss within 30 days. <sup>17</sup> Control foams had 100% mass loss within 12 weeks, and 30% DEG foams had 23% mass remaining after 14 weeks. <sup>21</sup> This data was collected on samples that were subjected to washing and drying procedures at each time point and returned to media for further testing at later time points. <sup>13,15,16,19,49</sup> This process is referred to as the "Literature Method."

While analyzing in vivo mass loss profiles, it was observed that control foams had 62% mass remaining, 30% DEG foams had 80% mass remaining, and 30% NTA-DEG had  $\sim\!\!29\%$  mass remaining after 12 weeks, Figure 3. While the general trends in mass loss rates remained the same, with 30% NTA-DEG undergoing the fastest degradation, followed by control foams with an intermediate degradation rate, and 30% DEG undergoing the slowest degradation, the overall degradation rates were much slower in vivo compared to previously observed in vitro degradation rates measured under presumed "real-time" conditions.

To address this issue, a parallel study was carried out to find testing conditions that could more closely correlate in vitro and in vivo degradation. In this "Optimized Method," multiple concentrations of  $H_2O_2$  were employed, and separate sacrificial samples were used to record mass loss at each time point to better mimic in vivo testing and reduce effects of washing/drying on later measurements. At each time point, the sacrificial sample was removed from the degradation media, rinsed in 70% ethanol, dried, weighed, and characterized. The sacrificial samples were not returned to the study after characterization.

Significant differences were observed between the degradation profiles obtained in 3% H $_2$ O $_2$  using the "Literature Method" and the "Optimized Method," Figure 2A. Faster degradation was observed in the

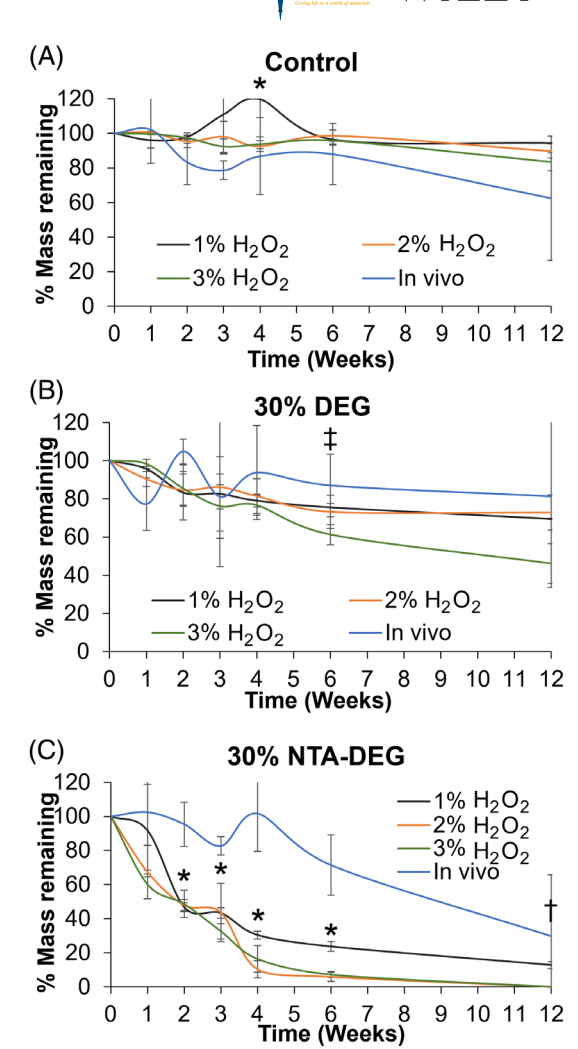


**FIGURE 3** Comparison between in vitro (n=3) and in vivo (n=5) mass loss profiles of (A) control, (B) 30% diethylene glycol (DEG), and (C) 30% nitrilotriacetic acid (NTA)-DEG foams. In vitro degradation was carried out in varying concentrations of  $H_2O_2$  (1%, 2%, and 3%). In vivo degradation data was collected after subcutaneous implantation in rats over 12 weeks. Mean  $\pm$  standard deviation is displayed. \*p < .05 between all in vitro measurements and in vivo measurement at same time point. †p < .05 between 2% and 3%  $H_2O_2$  measurements and in vivo measurement at same time point.

"Literature Method," which was attributed to physical erosion experienced by samples due to repeated washing and drying procedures at each time point. These physical forces were minimized in the 'Optimized Method,' as the samples were not subjected to multiple wash/dry cycles over time. SEM micrographs of samples characterized using the 'Optimized Method' demonstrate improved pore morphology retention after 6 weeks compared with 'Literature Method' samples, Figure 2B. No notable differences were seen between spectroscopic and thermal analyses of samples subjected to the two different methods, Figure 2C,D. This result indicates the validity of the hypothesis that changing testing procedures reduced undesired physical erosion and did not alter the chemical degradation process of the polymer network.

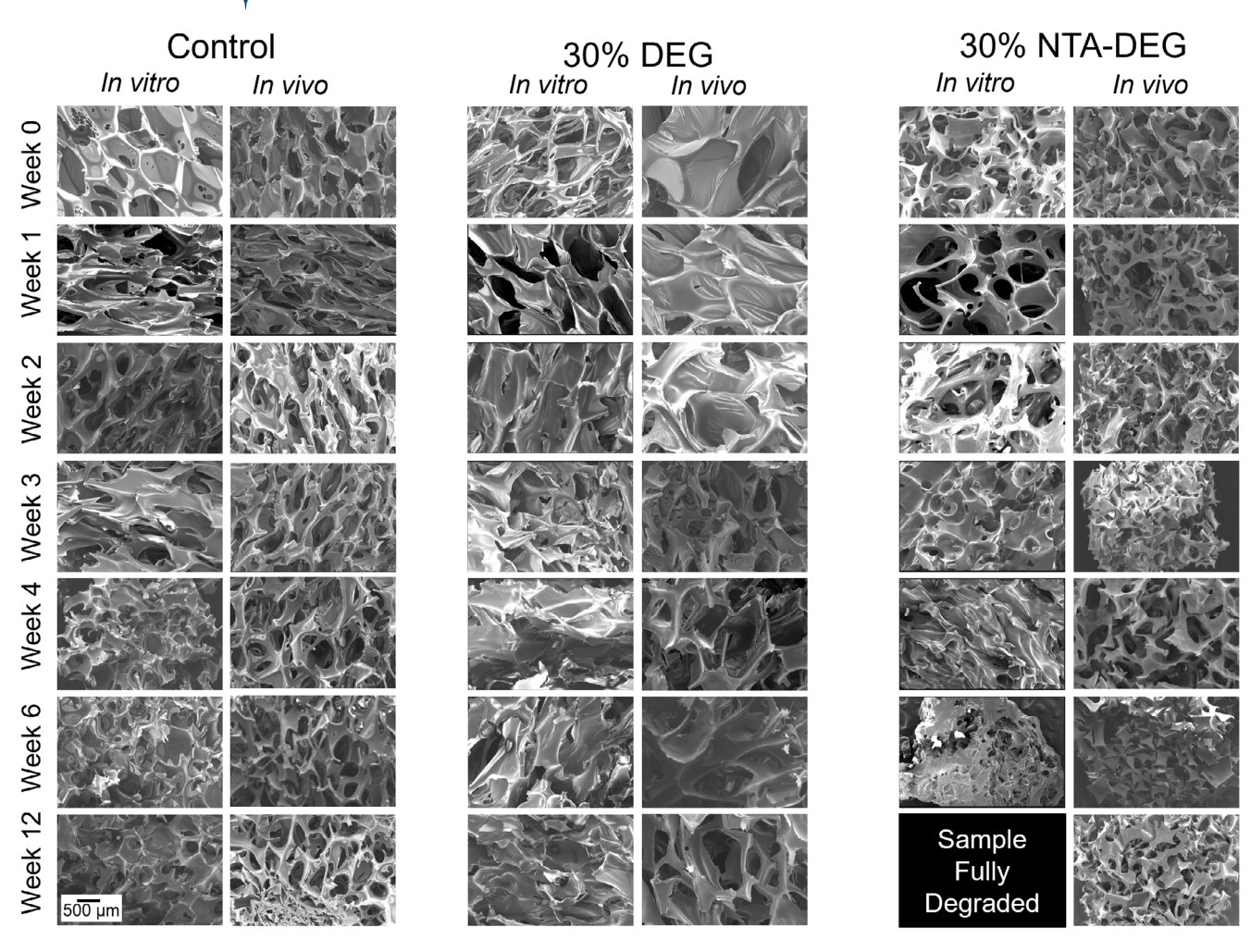


**FIGURE 4** Analysis of pore morphology via scanning electron microscopy of samples undergoing in vitro degradation (Control in 3%  $H_2O_2$ , 30% diethylene glycol (DEG), and 30% nitrilotriacetic acid (NTA)-DEG in 1%  $H_2O_2$ ¬) and in vivo degradation (subcutaneous implantation in rats). The scale bar of 500  $\mu$ m applies to all images

# 3.3.2 | Mass loss

After ensuring that unwanted effects of additional physical erosion were minimized and that pre- and post-explantation processing was accounted for (Figures S1, S2), the optimized method was employed with varying concentrations of  $\rm H_2O_2$  to determine in vitro conditions that best mimic in vivo degradation for each composition. According to ISO 10993-13,  $\rm H_2O_2$  is reported to have comparable levels of reactive oxygen species (ROS) found in wound sites. However,  $\rm H_2O_2$  has a higher stability compared to other ROS, and it can more easily penetrate through sample membranes and tissues and remain within samples for longer time frames. Thus it is likely that  $\rm 3\%~H_2O_2$  provides higher levels of degradative species compared to ROS levels in vivo, and we therefore chose to characterize degradation in 1 and  $\rm 2\%~H_2O_2$  to enable better comparison between in vitro and in vivo studies, Figure 3.

We found that the  $H_2O_2$  solution that best mimicked in vivo degradation conditions depended on the material chemistry and hydrophobicity. The general trends in degradation rates in each medium were still the same, with the order of degradation rate as follows: 30% NTA-DEG > Control >30% DEG. The mass loss profile for control

foams obtained using 3%  $H_2O_2$  was a close match to that obtained in vivo, Figure 3A, with statistically comparable measurements taken out to 12 weeks of degradation. This result is attributed to the oxidative degradation mechanism of control foams via scission of tertiary amines and high hydrolytic stability, as described in previous work.  $^{13}$ 

Compared to control foams, 30% DEG foams are slightly more hydrophilic, which enables faster water penetration and could increase access of ROS to polymer chains to accelerate degradation. Additionally, DEG foams are susceptible to oxidative degradation of both tertiary amines in HPED and ether groups in DEG. However, ether linkages can undergo parallel crosslinking during oxidation. This property may lead to simultaneous chain scission and crosslinking to slow the degradation process, which complicates degradation estimations and slowed overall degradation rates in this SMP foam system. Thus, lower concentrations of 1 and 2%  $\rm H_2O_2$  most closely mimicked in vivo degradation profiles for 30% DEG foams, as shown in Figure 3B, with statistically comparable measurements at all time points except week 6 (p value = .022).

Similarly, a lower concentration of  $1\%\ H_2O_2$  proved to have a closer match to in vivo degradation profiles for  $30\%\ NTA\text{-DEG}$  foams, as shown in Figure 3C, but in vitro degradation was significantly faster

than in vivo degradation after 2 weeks for all  $H_2O_2$  concentrations, except for week 12, where 1%  $H_2O_2$  samples had a comparable mass to the in vivo samples. The relatively hydrophilic 30% NTA-DEG foams are susceptible to hydrolytic cleavage of NTA-DEG esters, oxidation of tertiary amines in HPED, oxidative cleavage and/or crosslinking of ether groups in DEG, and enzymatic degradation of esters by lipase. In addition to the possible effects of hydrophilicity mentioned above, ester hydrolysis forms a carboxylic acid byproduct that can catalyze hydrolysis to increase the overall degradation rate in aqueous conditions. We hypothesize that samples were protected from reactive agents by fibrous encapsulation after in vivo implantation to slow degradation rates relative to in vitro measurements. For further analysis, data collected from degradation in 3%  $H_2O_2$  was used to analyze control foams, and data collected from incubation in 1%  $H_2O_2$  was used to analyze 30% DEG and 30% NTA-DEG foams.

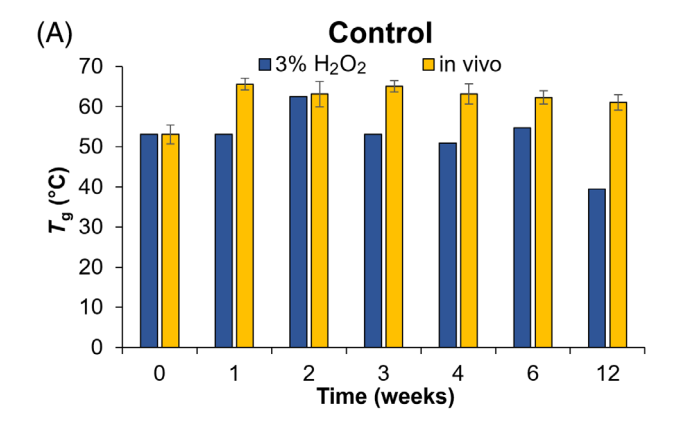
#### 3.3.3 | Physical analysis: pore morphology

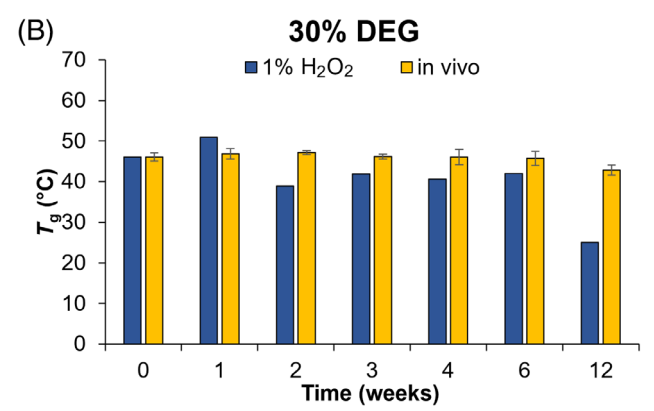
Overall, pore morphology was maintained across all formulations during in vivo degradation, Figure 4. Control foams lost their pore structure with visible strut breakage after 4 weeks of in vitro degradation in 3% H<sub>2</sub>O<sub>2</sub>. During in vivo degradation, control foams had some strut breakage beginning at week 6, but overall pore structure was maintained throughout 12 weeks, and no loss in pore structure was seen. Amongst 30% DEG foams, increased pore stability was observed compared to control foams, as expected. During in vitro degradation in 1% H<sub>2</sub>O<sub>2</sub>, overall pore structure was lost after 6 weeks, with some breakage in pore struts observed at week 4. Some strut breakage was observed after 6 and 12 weeks of in vivo degradation, but no loss in overall pore structure was seen in 30% DEG foams in vivo degradation. The fastest loss in pore structure and earliest occurrence of strut breakage (week 2) was observed in 30% NTA-DEG during in vitro degradation in 1% H<sub>2</sub>O<sub>2</sub>, and complete pore collapse was observed from week 4 onwards. However, during in vivo degradation, overall pore structure and interconnectivity were maintained throughout 12 weeks with some strut breakage beginning in week 2 onwards.

The maintenance of pore structure and interconnectivity across all formulations over the entire 12 weeks of implantation shows that SMP foams maintain their structural integrity in vivo and could therefore serve as a stable scaffold for uniform tissue ingrowth and vascularization in long-term implantation applications. While mechanical properties were not characterized over time in these studies, we hypothesize that these changes in foam structure would be accompanied by a reduction in stiffness and strength over time. In regenerative medicine applications, these changes in mechanical properties would enable a gradual transfer of load from the implanted scaffold to the surrounding tissue as it regenerates.<sup>55</sup>

# 3.3.4 | Chemical analysis: thermal and spectroscopic properties

Analysis of  $T_{\rm g}$  during degradation provides an estimate of the relative crosslink density over time to analyze surface vs. bulk erosion, where





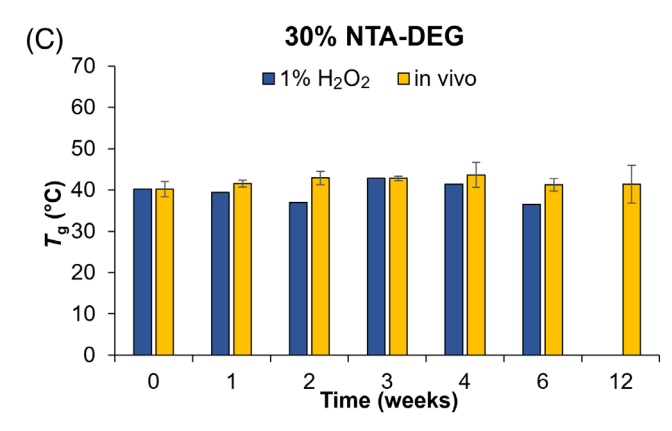


**FIGURE 5** Glass transition temperature ( $T_g$ ) of (A) Control, (B) 30% DEG, and (C) 30% nitrilotriacetic acid (NTA)-diethylene glycol (DEG) samples during in vitro degradation (blue bars) in 3%  $H_2O_2$  (Control) or 1%  $H_2O_2$  (30% DEG and 30% NTA-DEG) (n=1) and in vivo degradation (yellow bars) in subcutaneous pockets in rats (n=3). No statistical significance was observed over time for any formulation after in vivo implantation (p>.05)

surface erosion would result in retention of sample  $T_{\rm g}$  over time, and bulk erosion would cause decreases in  $T_{\rm g}$ . Overall,  $T_{\rm g}$  was maintained throughout the majority of the degradation both in vitro and in vivo, as shown in Figure 5. A large reduction in  $T_{\rm g}$  was observed for control and 30% DEG foams at 12 weeks of in vitro degradation. For 30% NTA-DEG foams, the sacrificial sample was completely degraded by week 12, indicated by a lack of data point here. No significant reductions in  $T_{\rm g}$  were measured over time in the in vivo degradation samples. Maintenance of  $T_{\rm g}$  over the entire 12 weeks of implantation can

3524965, 2023, 5, Downloaded from https://onlinelibrary.wiley.com/doi/10.1002/jbm.a.37504 by Test, Wiley Online Library on [02/06/2023]. See the Terms and Conditions (https://onlinelibrary.wiley.com/terms-and-conditions) on Wiley Online Library for rules of use; OA articles are governed by the applicable Creative Commons Licenses

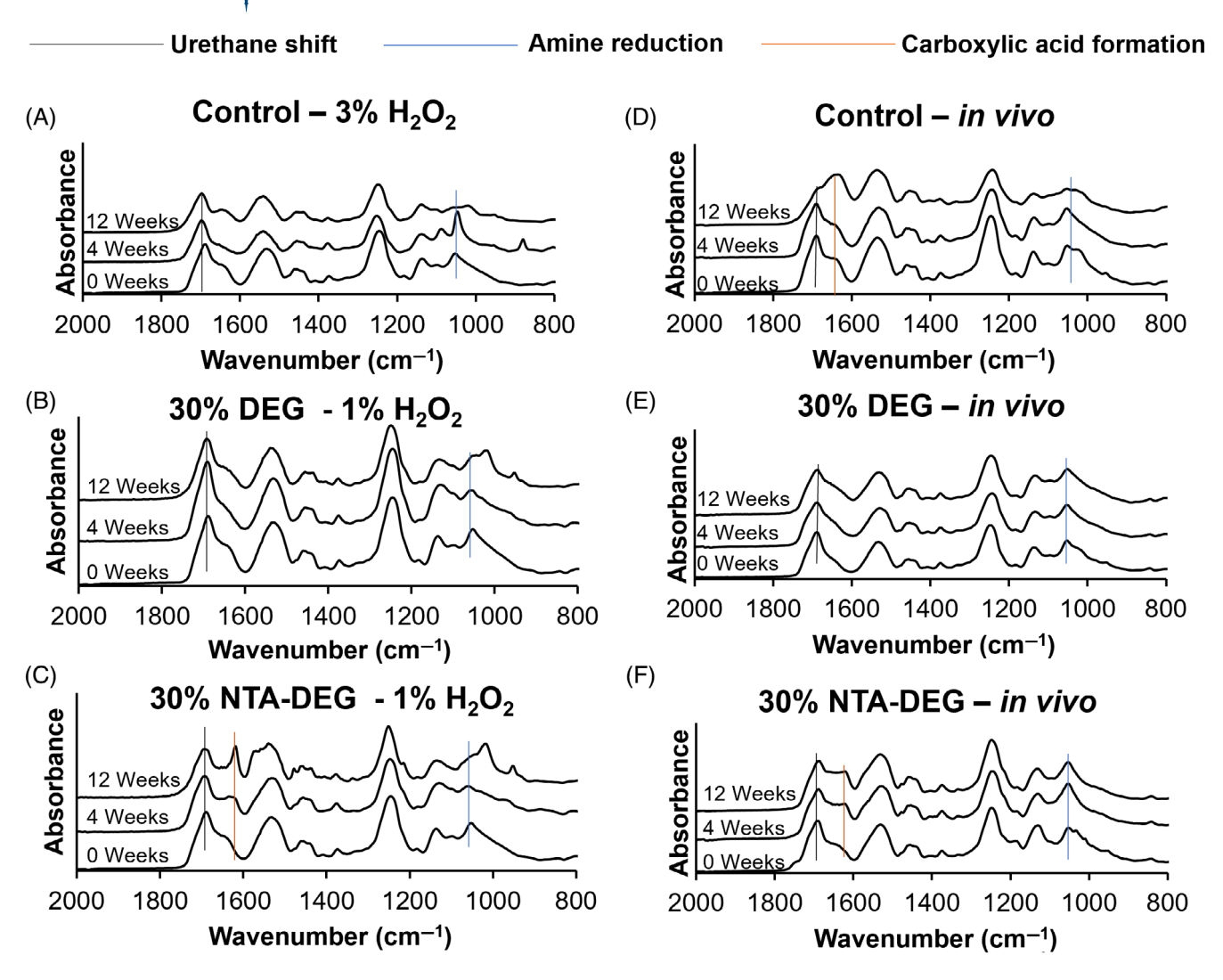


**FIGURE 6** Spectroscopic analysis of shape memory polymer (SMP) foams undergoing degradation at 0, 4, and 12 weeks. (A–C) Control, 30% diethylene glycol (DEG) and 30% nitrilotriacetic acid (NTA)-DEG undergoing in vitro degradation, respectively. (D–F) |Control, 30% DEG, and 30% NTA-DEG undergoing in vivo degradation, respectively

be attributed to high reactivity and low stability of ROS, which limits their diffusion through the sample membranes and restricts degradation to a surface level.

A shift in the urethane peak from 1680<sup>-</sup> to 1688 cm<sup>-1</sup> and a reduction in the tertiary amine peak at 1050 cm<sup>-1</sup> was observed in all foams during degradation, Figure 6. These changes are attributed to oxidative degradation of tertiary amines in the monomers (HPED, TEA, and NTA-DEG) to form primary amines as previously described.<sup>13</sup> A carboxylic acid peak appeared on control foams at 12 weeks of in vivo degradation, Figure 6D. This change is due to the reduction of tertiary amines in control foams to form primary amines and carboxylic acids.<sup>13</sup> Amongst 30% NTA-DEG foams, a stronger carbonyl peak appears at 1730 cm<sup>-1</sup> during in vitro degradation compared to that in vivo, Figure 6C,F. This change is attributed to the combination of oxidative degradation of tertiary amines and hydrolytic degradation of esters that occurs in these foams in 1% H<sub>2</sub>O<sub>2</sub>, and

the relative changes correlate with the observed increased in vitro mass loss in these foams.

# 3.3.5 | General considerations for correlating in vitro and in vivo degradation

Degradation rates are dependent on surface chemistry, surface area, and porosity, which affect the ability of degradative species to access polymer chains. <sup>56–58</sup> It is also important to consider implant location and its impact on degradation. Intramuscular degradation rates are higher than subcutaneous degradation rates, a trend that has been consistently observed using different polymer compositions and varying animal models. <sup>59–61</sup> With the current SMP foam system, degradation is faster after intravenous implantation in comparison with subcutaneous implantation. After 90 days of implantation in an

**FIGURE 7** Cytocompatibility of foams. (A) Cytocompatibility of 3T3 mouse fibroblasts over 0, 24, and 72 h (n = 3) of indirect contact with foam samples. (B) Dose–response curve of fully degraded foam solutions and 2% hydrogen peroxide solution control after neutralization with catalase (n = 3). Mean  $\pm$  standard deviation displayed. \*p < .05 relative to positive control

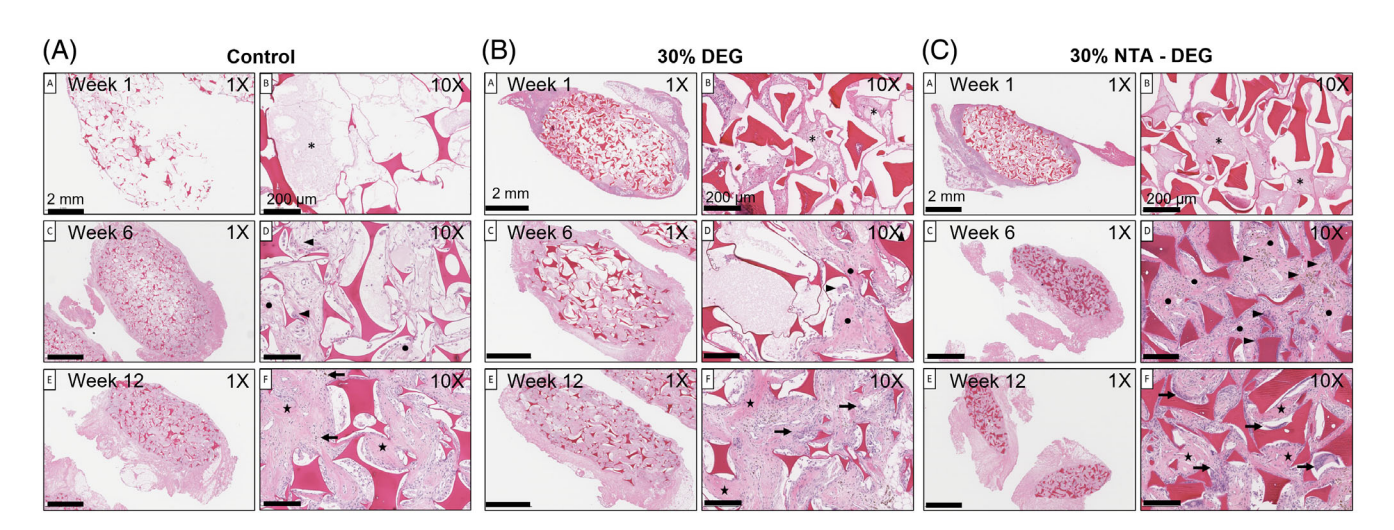


FIGURE 8 Histological assessment of explanted (A) Control, (B) 30% diethylene glycol (DEG), and (C) 30% nitrilotriacetic acid (NTA)-DEG foams at 1, 6, and 12 weeks. Scale bar labels apply to all images in a given column. In control foams, central regions progress from significant fibrin (asterisk) and minimal cellularity at 1 week, to collagen deposition (dots) and cellular infiltration (mostly macrophages, arrowheads) at 6 weeks, to a healing phase consisting of more prominent collagen deposition (stars) and increased hemosiderin-laden macrophages (arrows) at 12 weeks. In 30% DEG foams, central regions exhibit abundant fibrin (asterisks) and mild cellularity at 1 week. At 6 weeks, collagen deposition (dots) and cellularity (mainly macrophages, arrowheads) increase. A slightly denser extracellular matrix (stars) with increased cellularity (arrows) is seen at 12 weeks. In 30% NTA-DEG foams, central areas have abundant fibrin (asterisks) and minimal cellularity at 1 week. Collagen deposition (dots) and increased inflammatory cells (mostly macrophages, arrowheads) are seen at 6 weeks. At 12 weeks, fewer inflammatory cells (arrows) in a fibrous background (stars) are detected

aneurysm model, 40% mass loss of control foams was previously measured, compared with only 30% mass loss at 84 days in the current subcutaneous implant study. Thus, for a given formulation (control foams), degradation may vary based on implant location, and in vitro conditions should be altered to account for those potential changes. Specifically, a lower concentration of  $\rm H_2O_2$  is needed in vitro to predict slower subcutaneous in vivo degradation profiles than would be required to estimate intravenous degradation rates.

Even though the optimized method presented here better mimics the in vivo degradation process, the media required to accurately predict in vivo degradation is highly complex and depends on the chemical composition of the material under consideration. The foams that undergo only oxidative degradation can be more accurately modeled in vitro in H<sub>2</sub>O<sub>2</sub>, allowing for predictions of in vivo degradation rates prior to implantation. Ester-containing foams (30% NTA-DEG) undergo degradation via multiple potential mechanisms: hydrolytic and/or enzymatic degradation of esters and oxidative degradation of ethers and tertiary amines. Furthermore, the breakdown of esters and tertiary amines to form carboxylic acids lowers the pH, which can further catalyze hydrolytic degradation.<sup>54</sup> It is possible that this autocatalysis from ester hydrolysis combined with limited space for acidic byproducts to escape in the vials accelerated in vitro degradation in these foams. Additionally, the presence of fibrous tissue likely restricted diffusion of degradative species into foams in vivo. While



**TABLE 4** Cell types within each explant sample throughout 12 weeks of in vivo implantation (n = 9)

		Control					
		Week 1	Week 2	Week 3	Week 4	Week 6	Week 12
Acute	Neutrophils	0.2	0.4	7.9	_	-	-
inflammation	Eosinophils	_	_	_	_	-	_
	Macrophages	2.7	9.4	11.1	16	23.2	35
	Erythrophagocytosis	_	_	_	_	_	_
Chronic	Hemosiderin-laden macrophages	-	-	-	-	3	9.4
inflammation	Plasma cells	-	_	_	_	-	_
	Lymphocytes	-	0.4	0.1	0.4	0.6	1.8
	Giant cells	-	0.2	0.2	1	1.4	0.2
	Collagen (low, intermediate and high density)	Absent	Low	Low	Intermediate	Low- Intermediate	Intermediat
	Debris score (cellular necrosis, fibrin, hemorrhage)	Severe	Severe	Severe	Minimal	Mild	Mild
	Tissue response score (Jessen 2019)	6	5	5	1	2	2
		30% DI	EG				
		Week 1	Week 2	Week 3	Week 4	Week 6	Week 12
Acute	Neutrophils	2.6	0.4	0.2	-	-	-
inflammation	Eosinophils	0.6	-	0.3	0.1	0.1	-
	Macrophages	5.1	5.7	23.2	13.5	14.2	18.7
	Erythrophagocytosis	-	0.2	0.2	-	-	-
Chronic	Hemosiderin-laden macrophages	-	-	5.9	1.3	3.8	10.1
inflammation	Plasma cells	-	-	0.2	-	0.4	-
	Lymphocytes	0.8	0.3	0.2	0.4	0.7	0.6
	Giant cells	-	-	0.9	0.6	1	0.2
	Collagen (low, intermediate and high density)	Low	Low	Intermediate	Intermediate- high	Intermediate	Intermediat high
	Debris score (cellular necrosis, fibrin, hemorrhage)	Severe	Severe	Minimal	Mild	Moderate	Minimal
	Tissue response score (Jessen 2019)	5	4	2	1	2	2
		30% N	TA-DEG				
		Week 1	Week 2	Week 3	Week 4	Week 6	Week 12
Acute	Neutrophils	1.9	0.3	0.3	0.3	-	-
inflammation	Eosinophils	0.4	0.2	0.2	0.4	1.1	0.1
	Macrophages	1.2	21.6	12.2	28.7	42	25.9
	Erythrophagocytosis	-	-	-	-	-	-
	Li y tili opilagocytosis						
	Hemosiderin-laden macrophages	-	-	7	7	12.6	2.8
Chronic inflammation	, , ,	-	- 0.1	7	7	12.6	2.8
	Hemosiderin-laden macrophages	- - -				12.6 - 1	
	Hemosiderin-laden macrophages Plasma cells	- - -	0.1	-	-	-	-
Chronic inflammation	Hemosiderin-laden macrophages Plasma cells Lymphocytes	- - - - Absent	0.1 0.2 0.9	- 0.2 0.4 Low	- 2.2 0.4 Intermediate	- 1	- 0.7
	Hemosiderin-laden macrophages Plasma cells Lymphocytes Giant cells Collagen (low, intermediate and high	- Absent	0.1 0.2 0.9 Low	- 0.2 0.4 Low	- 2.2 0.4 Intermediate	- 1 0.9 Intermediate	- 0.7 0.8



#### TABLE 4 (Continued)

Tissue response score	
1	Mid-stage healing to healed
2	Mid-stage healing
3	Early to mid-stage healing
4	Early-stage healing
5	Residual blood to early stage healing
6	Residual blood

Note: Scores associated with tissue responses are shown above.

the NTA-DEG foam system is complicated to model in vitro, this work provides a significant improvement over previously published work that correlates in vitro and in vivo degradation profiles of SMP foams. This data presents a framework for assuming that materials that that undergo both hydrolysis and oxidation will degrade more slowly in vivo, which could aid in rational selection of formulations for animal testing. Overall, these studies provide a framework for the selection of in vitro conditions that better mimic implantation conditions to enable a more efficient screening of biomaterials before in vivo characterization.

#### 3.4 | Biological interactions

# 3.4.1 | Cytocompatibility of foams and degradation byproducts

All foams had cytocompatibility >80% after indirect incubation with 3T3 mouse fibroblasts for 72 h, Figure 7A. Cytocompatibility >75% is considered acceptable for medical devices according to ISO 10993-5 standards.<sup>34</sup> Once initial foam cytocompatibility was confirmed, cells were exposed to fully degraded foam solutions to evaluate safety of degradation byproducts. Degradation byproducts had ~25%-50% cytocompatibility when tested without any dilution, while the positive control that contained 2% H<sub>2</sub>O<sub>2</sub> neutralized by catalase had >75% cytocompatibility. However, a  $2\times$  dilution of the byproducts increased viability to  $\sim$ 60%-75%, and a  $4\times$  dilution further increased cytocompatibility to  $\sim$ 71%-100%. All further dilutions had ≥100% viability, Figure 7B. The nondiluted solutions represent a case wherein the surrounding cells would be exposed to all the degradation byproducts at once, which is not likely to occur during in vivo degradation, as the foams gradually degrade over time and degradation byproducts would diffuse away from the implant site and get eliminated from the body. An increase in cell viability with only a 2-4X dilution indicates that foam degradation would not cause cytotoxic concerns over the degradation time frame.

# 3.4.2 | Histological assessment

Overall, subcutaneous wounds reached a mid-healing stage regardless of foam implant type, Figure 8. Central regions of the control foam

implants had significant fibrin content and minimal cellularity at week 1, Figure 8A. By week 6, high levels of collagen deposition and cellular infiltration (primarily macrophages) were observed. A healing phase with more prominent collagen deposition and increased hemosiderinladen macrophages were seen at 12 weeks. After implantation of 30% DEG foams (Figure 8B), abundant fibrin presence and mild cellularity were observed at week 1, and increased collagen deposition and cellularity (primarily macrophages) were observed at week 6. A slightly denser extracellular matrix with increased cellularity was seen at week 12. Amongst the 30% NTA-DEG foams, Figure 8C, the central regions of the materials had minimum cellularity and abundant fibrin content at week 1. An increase in collagen deposition and inflammatory cells (mostly macrophages) was observed at week 6. At 12 weeks, slightly fewer inflammatory cells were detected in a fibrous background. The type of cells found within each explant tissue across the degradation time is summarized in Table 4. These results, taken together with the low measured toxicity of degradation byproducts, indicate that SMP foam scaffolds do not induce an undesired immune response during degradation, regardless of chemistry and degradation rate.

The average in vivo subcutaneous implant mass losses per day over the 84 days of implantation were estimated as  $0.34\% \pm 0.15\%$  for control foams,  $0.22\% \pm 0.04\%$  for 30% DEG foams, and  $0.83\% \pm 0.32\%$  for 30% NTA-DEG foams. Reductions in degradation rates were observed from week 6 to week 12, which correlated with the histological observations. Namely, as scar tissue is primarily made up of collagen, 62 the gradual observed increase in collagen deposition from low at week 1 to intermediate at week 6 and intermediate-high at week 12 indicates wound healing and fibrous tissue formation. This scar tissue around the implanted materials could shield the sample surfaces and limit ROS availability over time to slow degradation rates. Additionally, the decrease in macrophages over time indicates a lowered immune response with reduced ROS concentrations, thereby slowing degradation rates between weeks 6 and 12.

### 4 | CONCLUSIONS

Here, we have shown the ability to tune SMP foam degradation rates in vivo by altering monomer chemistry. The dry  $T_{\rm g}$ 's above 40°C, high shape fixity, and fast volume recovery allow for stable storage and quick administration of samples at desired implant locations. We



identified in vitro methods that better mimic in vivo degradation rates in comparison with previous studies. As degradation mechanisms get more complex in foams that degrade by both hydrolysis and oxidation, it is more difficult to model in vivo degradation using simple in vitro media. However, this information can still enable more accurate degradation rate predictions in future studies. This SMP foam system with tunable degradation rates can be used as a platform to design degradable scaffolds for future tissue regeneration applications.

#### **ACKNOWLEDGMENTS**

This material is based on research sponsored by U.S. Air Force under agreement number FA8650-18-2-6978. The U.S. Government is authorized to reproduce and distribute reprints for Governmental purpose notwithstanding any copyright notation thereon. The views and conclusions contained herein are those of the authors and should not be interpreted as necessarily representing the official policies or endorsements, either expressed or implied, of U.S. Air Force or the U.S. Government.

#### **DATA AVAILABILITY STATEMENT**

The data that support the findings of this study are available from the corresponding author upon reasonable request.

#### ORCID

Anand Utpal Vakil https://orcid.org/0000-0002-6303-8562

Natalie Marie Petryk https://orcid.org/0000-0002-5352-8365

Maryam Ramezani https://orcid.org/0000-0002-5870-3097

Mary Beth Browning Monroe https://orcid.org/0000-0003-4540-5303

#### REFERENCES

- Peterson GI, Dobrynin AV, Becker ML. Biodegradable shape memory polymers in medicine. Adv Healthc Mater. 2017;6(21):1700694.
- Dueramae I, Nishida M, Nakaji-Hirabayashi T, Matsumura K, Kitano H. Biodegradable shape memory polymers functionalized with anti-biofouling interpenetrating polymer networks. J Mater Chem B. 2016;4(32):5394-5404.
- 3. Joo YS, Cha JR, Gong MS. Biodegradable shape-memory polymers using polycaprolactone and isosorbide based polyurethane blends. *Mater Sci Eng C*. 2018;91:426-435.
- Guo Y, Lv Z, Huo Y, et al. A biodegradable functional waterresponsive shape memory polymer for biomedical applications. J Mater Chem B. 2019;7(1):123-132.
- Tsujimoto T, Takayama T, Uyama H. Biodegradable shape memory polymeric material from epoxidized soybean oil and polycaprolactone. *Polymers*. 2015;7(10):2165-2174.
- Xie M, Wang L, Ge J, Guo B, Ma PX. Strong electroactive biodegradable shape memory polymer networks based on star-shaped Polylactide and aniline trimer for bone tissue engineering. ACS Appl Mater Interfaces. 2015;7(12):6772-6781.
- Deng Z, Guo Y, Zhao X, et al. Stretchable degradable and electroactive shape memory copolymers with tunable recovery temperature enhance myogenic differentiation. Acta Biomater. 2016;46: 234-244.
- 8. Marshall A, Irvin C, Barker T, Sage K, Hauch E, Ratner B. *Biomaterials* with *Tightly Controlled Pore Size that Promote Vascular in-Growth*. American Chemical Society; 2004.
- Hollister SJ. Porous Scaffold Design for Tissue Engineering. Nat Mat. 2005;4(7):518-524.

- Xie H, Deng X-Y, Cheng C-Y, Yang K-K, Wang Y-Z. New strategy to access dual-stimuli-responsive triple-shape-memory effect in a nonoverlapping pattern. *Macromol Rapid Commun.* 2017;38(4):1600664.
- Rodriquez JN, Clubb FJ, Wilson TS, et al. In vivo tissue responses following implantation of shape memory polyurethane foam in a porcine aneurysm model. J Biomed Mater Res A. 2014;102(5):1231-1242.
- Jessen SL, Friedemann MC, Mullen AE, et al. Micro-CT and histopathology methods to assess host response of aneurysms treated with shape memory polymer foam-coated coils versus bare metal coil occlusion devices. J Biomed Mater Res Part B: Appl Biomater. 2020; 108(5):2238-2249.
- Weems AC, Wacker KT, Carrow JK, Boyle AJ, Maitland DJ. Shape memory polyurethanes with oxidation-induced degradation: In vivo and in vitro correlations for endovascular material applications. *Acta Biomater*. 2017;59:33-44.
- Singhal P, Small W, Cosgriff-Hernandez E, Maitland DJ, Wilson TS. Low density biodegradable shape memory polyurethane foams for embolic biomedical applications. *Acta Biomater*. 2014;10(1):67-76.
- Weems AC, Easley A, Roach SR, Maitland DJ. Highly cross-linked shape memory polymers with tunable oxidative and hydrolytic degradation rates and selected products based on succinic acid. ACS Appl Bio Mater. 2019;2(1):454-463.
- Jang LK, Fletcher GK, Monroe MBB, Maitland DJ. Biodegradable shape memory polymer foams with appropriate thermal properties for hemostatic applications. J Biomed Mater Res Part A. 2020;108:1281-1294.
- Vakil AU, Petryk NM, Shepherd E, et al. Shape memory polymer foams with tunable degradation profiles. ACS Appl Bio Mater. 2021; 4(9):6769-6779.
- Weems AC, Carrow JK, Gaharwar AK, Maitland DJ. Improving the oxidative stability of shape memory polyurethanes containing tertiary amines by the presence of isocyanurate triols. *Macromolecules*. 2018; 51(22):9078-9087.
- Hasan SM, Fletcher GK, Monroe MBB, Wierzbicki MA, Nash LD, Maitland DJ. Shape memory polymer foams synthesized using glycerol and Hexanetriol for enhanced degradation resistance. *Polymers*. 2020:12(10):2290.
- Weems AC, Wacker KT, Maitland DJ. Improved oxidative biostability of porous shape memory polymers by substituting triethanolamine for glycerol. J Appl Polym Sci. 2019:136(35):47857.
- Vakil AU, Petryk NM, Shepherd E, Monroe MBB. Biostable shape memory polymer foams for smart biomaterial applications. *Polymers*. 2021;13(23):4084.
- Rodriguez JN, Yu YJ, Miller MW, et al. Opacification of shape memory polymer foam designed for treatment of intracranial aneurysms. Ann Biomed Eng. 2012;40(4):883-897.
- Horn J, Hwang W, Jessen SL, et al. Comparison of shape memory polymer foam versus bare metal coil treatments in an in vivo porcine sidewall aneurysm model. J Biomed Mater Res Part B: Appl Biomater. 2017;105(7):1892-1905.
- Standard I, Vibration M, Standard I, Cie SE, Standard I. ISO 10993-13 Identification and Quantification of Degradation Products from Polymeric Medical Devices. British Standard Institution; 2010.
- Jessen SL, Friedemann MC, Ginn-Hedman AM, et al. Microscopic assessment of healing and effectiveness of a foam-based peripheral occlusion device. ACS Biomater Sci Eng. 2020;6(5):2588-2599.
- Yang Q, Peng J, Guo Q, et al. A cartilage ECM-derived 3-D porous acellular matrix scaffold for in vivo cartilage tissue engineering with PKH26-labeled chondrogenic bone marrow-derived mesenchymal stem cells. *Biomaterials*. 2008;29(15):2378-2387.
- Wang F, Hu Y, He D, Zhou G, Yang X, Ellis E. Regeneration of subcutaneous tissue-engineered mandibular condyle in nude mice. J Cranio-Maxillofac Surg. 2017;45(6):855-861.
- Modulevsky DJ, Cuerrier CM, Pelling AE. Biocompatibility of subcutaneously implanted plant-derived cellulose biomaterials. PLoS One. 2016;11(6):e0157894.

- Klinge U, Junge K, Spellerberg B, Piroth C, Klosterhalfen B, Schumpelick V. Do multifilament alloplastic meshes increase the infection rate? Analysis of the polymeric surface, the bacteria adherence, and the in vivo consequences in a rat model. *J Biomed Mater* Res. 2002;63(6):765-771.
- 30. Laschke MW, Häufel JM, Thorlacius H, Menger MD. New experimental approach to study host tissue response to surgical mesh materials in vivo. *J Biomed Mater Res Part A*. 2005;74A(4):696-704.
- Neethling WML, Glancy R, Hodge AJ. Mitigation of calcification and cytotoxicity of a glutaraldehyde-preserved bovine pericardial matrix: improved biocompatibility after extended implantation in the subcutaneous rat model. J Heart Valve Dis. 2010;19(6):778-785.
- Padsalgikar A, Cosgriff-Hernandez E, Gallagher G, et al. Limitations of predicting in vivo biostability of multiphase polyurethane elastomers using temperature-accelerated degradation testing. J Biomed Mater Res Part B: Appl Biomater. 2015;103(1):159-168.
- Herting SM, Monroe MBB, Weems AC, et al. In vitro cytocompatibility testing of oxidative degradation products. J Bioact Compat Polym. 2021;36(3):197-211.
- ISO 10993-5:2009. Biological evaluation of medical devices—Part 5: tests for in vitro cytotoxicity. International Organization Standardization; 2009:34.
- Browning MB, Cereceres SN, Luong PT, Cosgriff-Hernandez EM.
   Determination of the in vivo degradation mechanism of PEGDA hydrogels. J Biomed Mater Res Part A. 2014;102(12):4244-4251.
- Wang Z, Wang S, Marois Y, Guidoin R, Zhang Z. Evaluation of biodegradable synthetic scaffold coated on arterial prostheses implanted in rat subcutaneous tissue. *Biomaterials*. 2005;26(35):7387-7401.
- Jansen K, Van Der Werff JFA, Van Wachem PB, Nicolai JPA, De Leij LFMH, Van Luyn MJA. A hyaluronan-based nerve guide: In vitro cytotoxicity, subcutaneous tissue reactions, and degradation in the rat. Biomaterials. 2004;25(3):483-489.
- Azab AK, Doviner V, Orkin B, et al. Biocompatibility evaluation of crosslinked chitosan hydrogels after subcutaneous and intraperitoneal implantation in the rat. J Biomed Mater Res Part A. 2007;83A(2):414-422.
- Christenson EM, Dadsetan M, Wiggins M, Anderson JM, Hiltner A. Poly(carbonate urethane) and poly(ether urethane) biodegradation: In vivo studies. J Biomed Mater Res Part A. 2004;69(3):407-416.
- Kim J, Dadsetan M, Ameenuddin S, Windebank AJ, Yaszemski MJ, Lu L. In vivo biodegradation and biocompatibility of PEG/sebacic acid-based hydrogels using a cage implant system. J Biomed Mater Res Part A. 2010;95(1):191-197.
- Zhang Z, Guidoin R, King MW, How TV, Marois Y, Laroche G. Removing fresh tissue from explanted polyurethane prostheses: which approach facilitates physico-chemical analysis? *Biomaterials*. 1995;16(5):369-380.
- Walthers CM, Nazemi AK, Patel SL, Wu BM, Dunn JCY. The effect of scaffold macroporosity on angiogenesis and cell survival in tissueengineered smooth muscle. *Biomaterials*. 2014;35(19):5129-5137.
- Xiao X, Wang W, Liu D, et al. The promotion of angiogenesis induced by three-dimensional porous beta-tricalcium phosphate scaffold with different interconnection sizes via activation of PI3K/Akt pathways. Sci Rep. 2015;5(1):9409.
- 44. Boyle AJ, Landsman TL, Wierzbicki MA, et al. In vitro and in vivo evaluation of a shape memory polymer foam-over-wire embolization device delivered in saccular aneurysm models. *J Biomed Mater Res Part B: Appl Biomater.* 2016;104(7):1407-1415.
- Landsman TL, Bush RL, Glowczwski A, et al. Design and verification of a shape memory polymer peripheral occlusion device. J Mech Behav Biomed Mater. 2016;63:195-206.
- Stefanopoulos PK, Hadjigeorgiou GF, Filippakis K, Gyftokostas D. Gunshot wounds: a review of ballistics related to penetrating trauma. J Acute Dis. 2014;3(3):178-185.
- Griffin MF, Leung BC, Premakumar Y, Szarko M, Butler PE. Comparison of the mechanical properties of different skin sites for auricular and nasal reconstruction. J Otolaryngol Head Neck Surg. 2017;46(1):1-6.

- 48. Karimi A, Rahmati SM, Navidbakhsh M. Mechanical characterization of the rat and mice skin tissues using histostructural and uniaxial data. *Bioengineered*. 2015;6(3):153-160.
- Weems AC, Li W, Maitland DJ, Calle LM. Polyurethane microparticles for stimuli response and reduced oxidative degradation in highly porous shape memory polymers. ACS Appl Mater Interfaces. 2018; 10(39):32998-33009.
- Dempsey DK, Carranza C, Chawla CP, et al. Comparative analysis of in vitro oxidative degradation of poly(carbonate urethanes) for biostability screening. J Biomed Mater Res Part A. 2014;102(10):3649-3665.
- ISO 10993-13:2010. Biological evaluation of medical devices—Part 13: identification and quantification of degradation products from polymeric medical devices. Accessed January 31, 2022. https://webstore.ansi.org/standards/iso/iso10993132010?gclid=Cj0KCQiArt6PBhCoAR IsAMF5wagszhYtuzxVwE8jKg6wiSllrgdvwj5DPhBODDPHDDRwNoHG Ajktlw0aAq4JEALw wcB.
- Dunnill C, Patton T, Brennan J, et al. Reactive oxygen species (ROS) and wound healing: the functional role of ROS and emerging ROSmodulating technologies for augmentation of the healing process. *Int* Wound J. 2017;14(1):89-96.
- Christenson EM, Anderson JM, Hiltner A. Oxidative mechanisms of poly(carbonate urethane) and poly(ether urethane) biodegradation: In vivo and in vitro correlations. J Biomed Mater Res Part A. 2004; 70(2):245-255.
- 54. Smith HA, Steele JH. The acid catalyzed hydrolysis of ethyl esters of aliphatic acids. *J Am Chem Soc.* 1941;63(12):3466-3469.
- Chan BP, Leong KW. Scaffolding in tissue engineering: general approaches and tissue-specific considerations. Eur Spine J. 2008; 17(4):467-479.
- Ghosh SC, Ngiam JSY, Seayad AM, Tuan DT, Chai CLL, Chen A. Copper-catalyzed oxidative amidation of aldehydes with amine salts: synthesis of primary, secondary, and tertiary amides. *J Org Chem.* 2012; 77(18):8007-8015.
- Bergstad K, Bäckvall JE. Mild and efficient Flavin-catalyzed H<sub>2</sub>O<sub>2</sub> oxidation of Tertiar amines to amine N-oxides. J Org Chem. 1998;63(19): 6650-6655.
- Martin JR, Gupta MK, Page JM, et al. A porous tissue engineering scaffold selectively degraded by cell-generated reactive oxygen species. *Biomaterials*. 2014;35(12):3766-3776.
- Olmo N, Turnay J, Gavilanes JG, Lizarbe MA, Herrera JI. Subcutaneous and intramuscular implantation of sepiolite-collagen complexes. J Mater Sci Mater Med. 1992;3(4):239-244.
- Beumer G, Vanblitterswijk C, Ponec M. Degradative behaviour of polymeric matrices in (sub)dermal and muscle tissue of the rat: a quantitative study. Biomaterials. 1994;15(7):551-559.
- Sabri F, Boughter JD Jr, Gerth D, et al. Histological evaluation of the biocompatibility of Polyurea Crosslinked silica aerogel implants in a rat model: a pilot study. *PLoS One*. 2012;7(12):e50686.
- 62. Madden JW, Peacock EE. Studies on the biology of collagen during wound healing. *Ann Surg.* 1971;174(3):511-520.

#### SUPPORTING INFORMATION

Additional supporting information can be found online in the Supporting Information section at the end of this article.

How to cite this article: Vakil AU, Petryk NM, Du C, et al. In vitro and in vivo degradation correlations for polyurethane foams with tunable degradation rates. *J Biomed Mater Res.* 2023;111(5):580-595. doi:10.1002/jbm.a.37504